ACS APPLIED MATERIALS & INTERFACES

Research Article

www.acsami.org

Regulation of the Biological Functions of Osteoblasts and Bone Formation by Zn-Incorporated Coating on Microrough Titanium

Xinkun Shen, Yan Hu, Gaoqiang Xu, Weizhen Chen, Kui Xu, Qichun Ran, Pingping Ma, Yarong Zhang, Jinghua Li, and Kaiyong Cai*

Key Laboratory of Biorheological Science and Technology, Ministry of Education College of Bioengineering, Chongqing University, Chongqing 400044, P. R. China

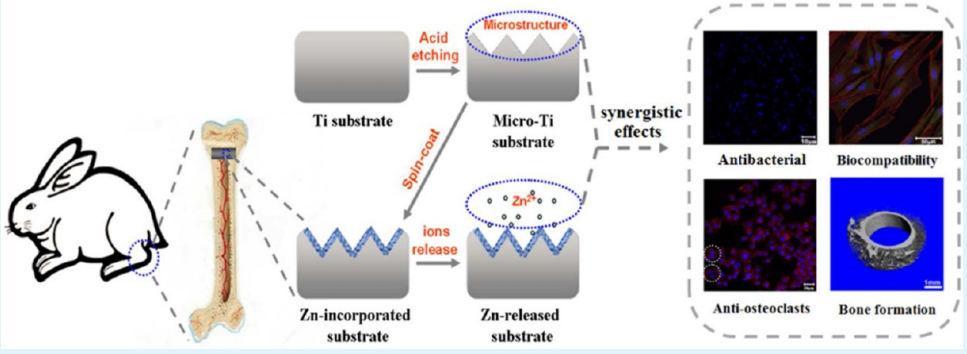

ABSTRACT: To improve the biological performance of titanium implant, a series of Zn-incorporated coatings were fabricated on the microrough titanium (Micro-Ti) via sol−gel method by spin-coating technique. The successful fabrication of the coating was verified by combined techniques of scanning electron microscopy, surface profiler, X-ray diffraction, X-ray photoelectron spectroscopy, and water contact angle measurements. The incorporated zinc existed as ZnO, which released Zn ions in a sustained manner. The Zn-incorporated samples (Ti−Zn0.08, Ti−Zn0.16, and Ti−Zn0.24) efficiently inhibited the adhesion of both Gram-positive (*Staphylococcus aureus*) and Gram-negative (*Pseudomonas aeruginosa*) bacteria. The *in vitro* evaluations including cell activity, alkaline phosphatase (ALP), mineralization, osteogenic genes expressions (Runx2, ALP, OPG, Col I, OPN, and OC), and tartrate-resistant acid phosphatase, confirmed that Ti−Zn0.16 sample was the optimal one to regulate the proliferation or differentiation for both osteoblasts and osteoclasts. More importantly, *in vivo* evaluations including Micro-CT analysis, push-out test, and histological observations verified that Ti−Zn0.16 implants could efficiently promote new bone formation after implantation for 4 and 12 weeks, respectively. The resulting material thus has potential application in orthopedic field.

KEYWORDS: *titanium, zinc, osteoblasts, osteogenesis, in vivo*

INTRODUCTION

Titanium (Ti) and its alloys were widely used as artificial joints, bone fixation devices, dental implants, etc. in orthopedic field, mainly due to their good mechanical properties, corrosion resistance, and biocompatibility.[1,2] Besides these advantages, some shortcomings (e.g., bioinertness, wears, etc.) of native titanium were found to hinder its osseointegration and even affect the long-term survival of Ti-based implants.[3,4] For practical application, bacterial infection is another clinical issue to be considered. The analysis showed that the annual infection rate for orthopedic implants was about 4.3% in the United States.[5] Once infection occurs, bacteria would form a biofilm onto the surface of implant to inhibit the osseointegration between implants and surrounding nature bone tissue.[6] It actually became an important reason that led to implantation failure.[7] Therefore, how to promote osseointegration and simultaneously inhibit bacterial adhesion of Ti-based implant became a research focus in the orthopedic field.

It is well-known that surface properties (e.g., chemistry, topography, texture, wettability, roughness, etc.) of a biomaterial play an important role in the regulation of the interactions between the biomaterial and cells/tissues.[8−11] As for a nondegradable implant, such as Ti-based implant, the initial and ultimate interactions with biological environments (e.g., protein absorption, blood, cells, tissues, etc.) only occur at its surface. Thus, how to surface engineer titanium so that to impose it with biofunctionality is essentially important either for fundamental research or for clinical application.

Because of its potential to induce the differentiation of bone related cells, the investigation on microrough titanium attracted more and more attention. For instance, Boyan et al. found that microrough titanium could promote the differentiation of

Received: July 25, 2014
Accepted: August 22, 2014
Published: August 22, 2014

dx.doi.org/10.1021/am5049338 | ACS Appl. Mater. Interfaces 2014, 6, 16426−16440

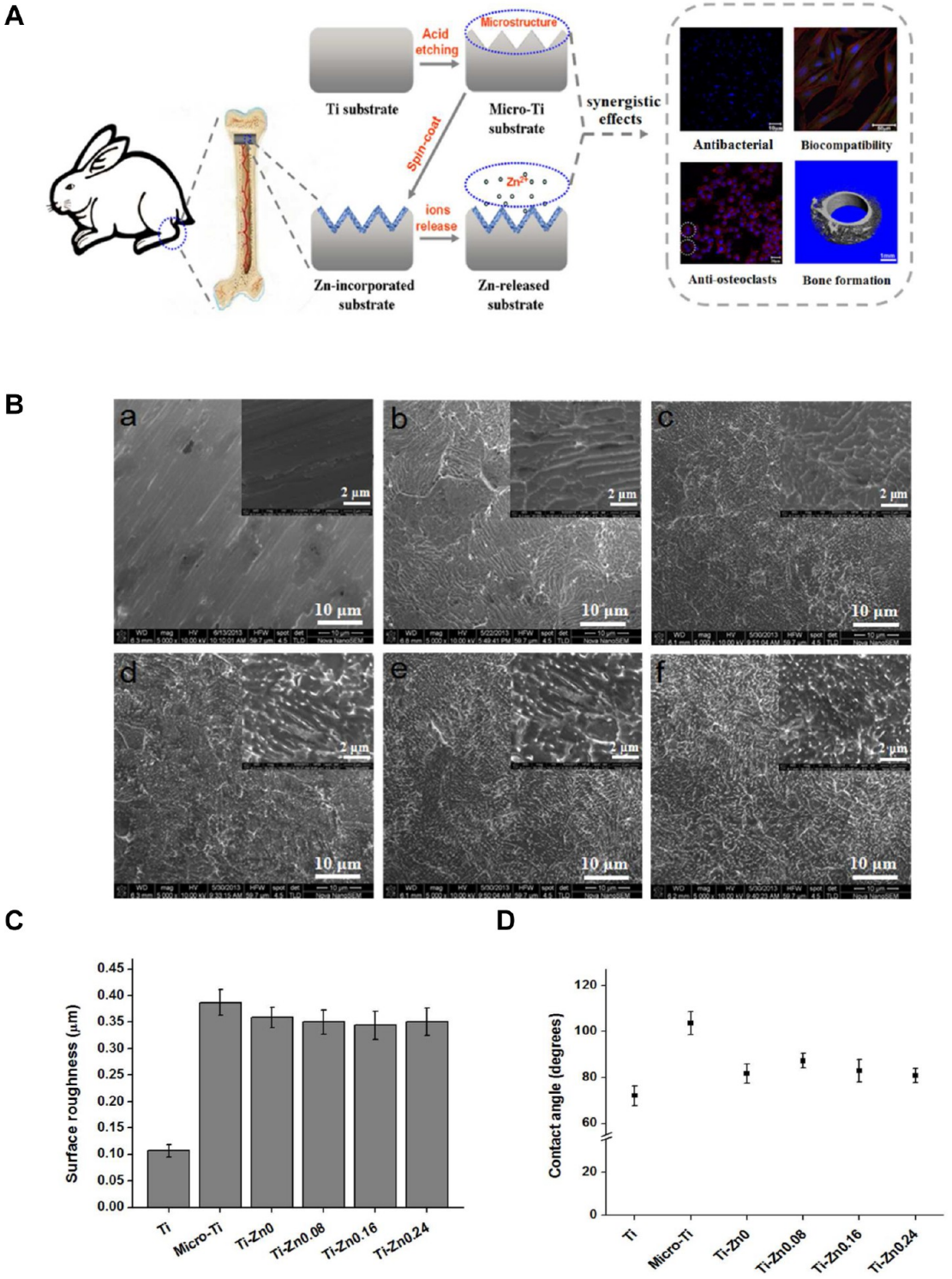

Figure 1. (A) Schematic illustration of this study; (B) SEM images of different substrates: (a) Ti, (b) Micro-Ti, (c) Ti−Zn0, (d) Ti−Zn0.08, (e) Ti−Zn0.16, and (f) Ti−Zn0.24; (C) surface roughness; and (D) water contact angles of different Ti substrates (n = 5).

mesenchymal stem cells (MSCs) toward osteoblasts.[12] And the osteoprotegerin (OPG) expression of osteoblasts could also be improved by the microstructured titanium.[13] Another study proved that microrough titanium could enhance the differentiation of SaOS-2 osteoblast-like cells.[14] However, other studies confirmed that microrough titanium had limitation to improve the proliferation of osteoblasts comparing with other biomaterials.[8,15]

To improve the biological functions of titanium, diverse strategies have been taken, such as micro/nano structures,[15,16] surface coatings,[17,18] chemical grafting,[8,19] ion implantation,[20] etc. For instance, previous studies had reported that the plastic deformation technologies, such as high-temperature calcination, high-pressure torsion, severe rolling, etc., could produce surface mico-nanostructure with nano/ultrafine grains, which in turn promoted cell adhesion, proliferation and differentiation.[21,22] In

dx.doi.org/10.1021/am5049338 | ACS Appl. Mater. Interfaces 2014, 6, 16426−16440

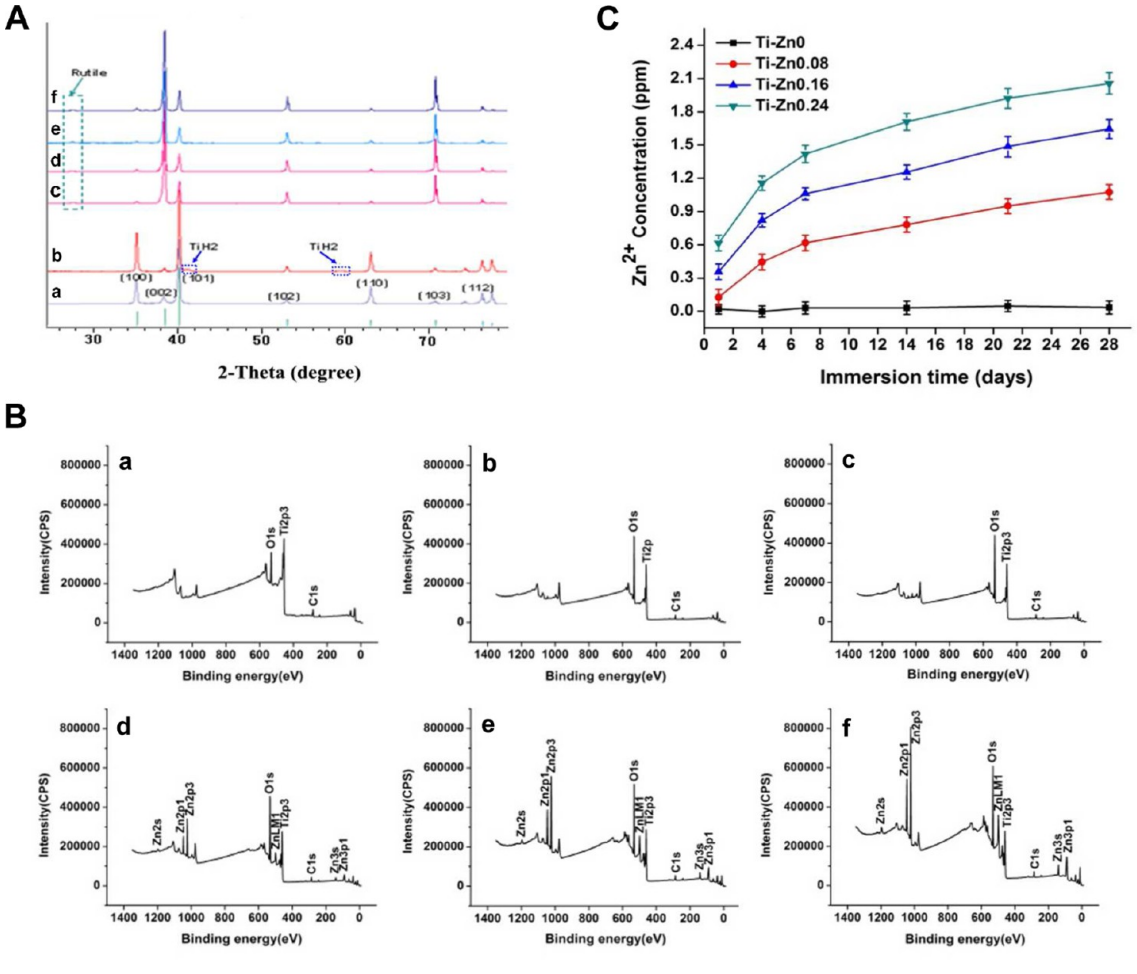

g

Samples	*Elemental content (at%)*			
	Ti	**O**	**C**	**Zn**
Ti	47.05±0.43	40.31±0.54	12.64±0.52	-
Micro-Ti	27.19±0.51	60.47±0.39	12.34±0.47	-
Ti-Zn0	25.52±0.47	62.61±0.41	11.87±0.63	-
Ti-Zn0.08	21.31±0.32	58.91±0.43	11.73±0.58	8.05±0.38
Ti-Zn0.16	18.64±0.46	55.68±0.57	12.14±0.49	13.54±0.49
Ti-Zn0.24	15.06±0.53	53.04±0.34	12.17±0.56	19.73±0.42

Figure 2. (A) X-ray diffraction patterns of (a) Ti, (b) Micro-Ti, (c) Ti−Zn0, (d) Ti−Zn0.08, (e) Ti−Zn0.16, and (f) Ti−Zn0.24; (B) XPS survey spectra of (a) Ti, (b) Micro-Ti, (c) Ti−Zn0, (d) Ti−Zn0.08, (e) Ti−Zn0.16, and (f) Ti−Zn0.24; (g) statistics of chemical compositions on the surface of different Ti substrates; and (C) zinc ion concentrations in SBF solution with immersion of Ti−Zn0, Ti−Zn0.08, Ti−Zn0.16, and Ti−Zn0.24 for 28 d.

another study, Esteban-Tejeda et al. proved that calcination could result in thermal expansion mismatch in the ZnO incorporated coatings, which played an important role in inhibiting the adhesion of *Escherichia coli*.[23] Thus, in this study, the combined technology of sol−gel and calcination were used to incorporate zinc with microrough titanium, so that to endow titanium with biofunctionality. The rationale to incorporate zinc was that it had many advantages, such as promoting cell growth,[20,24] anti−antibacterial adhesion,[24−26] etc.

Zinc is one of the necessary trace elements in human body. Zinc ions at appropriate dose have positive impact on cells growth.[20,27] However, a high dose of zinc ions would cause cytotoxicity, although the threshold concentration of zinc ions was dependent on cell types. For instance, Wätjen et al. reported that the mouse fibroblast cell line (NIH3T3) showed zinc toxicity at only 70 μM, while human lung adenocarcinoma cell line (A549) displayed zinc toxicity up to 600 μM.[28] Brauer et al. found that zinc concentrations between 50 and 300 μM could significantly increase the metabolic activity of MC3T3-E1 mouse osteoblast, and higher zinc content would lead to cytotoxicity.[29]

Zinc was also used as additive for the development of biomaterials. For instance, Boccaccini et al. added 0.125 to 1.0 wt % ZnO to biphasic β/α-tricalcium phosphate (TCP), and thus developed Zn−TCP with good interaction with osteoblasts.[30] Jayakumar et al. developed the chitosan hydro-

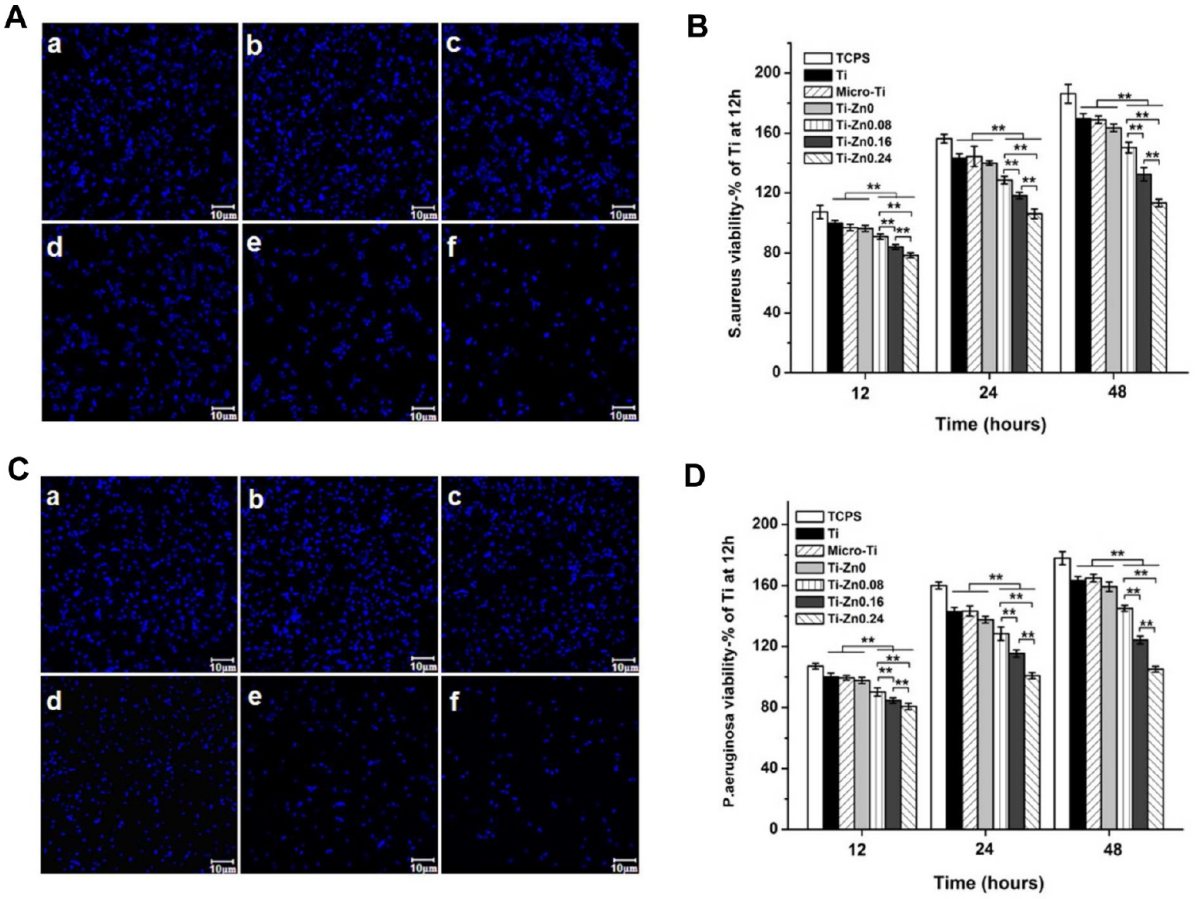

Figure 3. Antibacterial function assays: the representative fluorescence images of (A) *S. aureus* and (C) *P. aeruginosa* after culture for 12 h: (a) Ti, (b) Micro-Ti, (c) Ti−Zn0, (d) Ti−Zn0.08, (e) Ti−Zn0.16 and (f) Ti−Zn0.24; cell viability of (B) *S. aureus* and (D) *P. aeruginosa* adhered to different Ti substrates after culture for 12, 24, and 48 h (n = 6), respectively.

gel/nano ZnO composite that demonstrated good antibacterial property and interaction with fibroblasts.[31] Recently, Liu et al. found that Zn-implanted coatings had great potential to stimulate bone growth with the release zinc ions.[20] In another study, Hu et al. demonstrated that Zn-incorporated TiO_2 coatings could not only inhibit bacteria adhesion but also promote the proliferation and differentiation of MSCs.[24] Nevertheless, much work still needs to be investigated. For instance, as mentioned above, is there an optimal content of zinc as additive for titanium coating in an implant? Does the Zn-incorporated Ti have potential for the regulation of activity of osteoclasts? What is the preliminary mechanism behind? etc.

The present study has three purposes, as follows: (1) to fabricate a series of Zn-incorporated microrough titanium; (2) to screen those samples with optimal zinc content that would inhibit bacteria adhesion and improve biological functions (adhesion, proliferation, and differentiation) of osteoblasts/osteoclasts and to reveal the potential mechanism at molecular level; (3) to further investigate the osteogenesis of the screened Zn-incorporated Ti substrates *in vivo*.

■ RESULTS AND DISCUSSION

To achieve the goals of our vision (Figure 1A), we first fabricated the microrough surfaces on native Ti substrates by etching with 0.5% (v/v) hydrofluoric acid (HF) solution. Native Ti displayed rough surface morphology with discernible scratches, deriving from the polishing treatments (Figure 1B,a). After treatment with HF, micrometer-scale valleylike structure was observed on the surface of Ti substrates. The sample was designated as Micro-Ti. The distance between the valleys was ∼0.4−1.5 μm (Figure 1B,b). After sol−gel coating with $ZnCl_2$/EtOH/tetrabutyl titanate, the topological structures of the coated Ti substrates (Ti−Zn0, Ti−Zn0.08, Ti−Zn0.16, and Ti−Zn0.24) had only slight changes that the valleylike structures became slightly shallow comparing with Micro-Ti substrates (Figure 1B,c−f vs b). The result suggests that the thickness of the coating layer was ∼1−1.5 μm, comparable to the dimension of the valleylike structure of Micro-Ti. A previous study reported that the thickness of Zn layer was ∼5−10 μm; however, it was fabricated by plasma electrolytic oxidation.[24] Moreover, no delamination phenomenon was observed on all coated surfaces. The quantitative surface roughness (Rq) of the samples also demonstrated that there was only little difference between Micro-Ti and sol−gel-treated Micro-Ti samples (Figure 1C). As for sol−gel with calcination approach, a previous study confirmed that high-temperature calcination could induce the interface diffusion and reaction between TiO_2 film and aluminum alloy substrate, and the interface gradually blurred with the increasing of annealing temperature and time.[32] In another study, Gan et al. proved that there was a strong adhesion strength, which was enough to meet the needs of the clinical application at the interface of Ti6Al4V substrate and Ca−P coating, which were fabricated by the combined technology of sol−gel and calcination.[33]

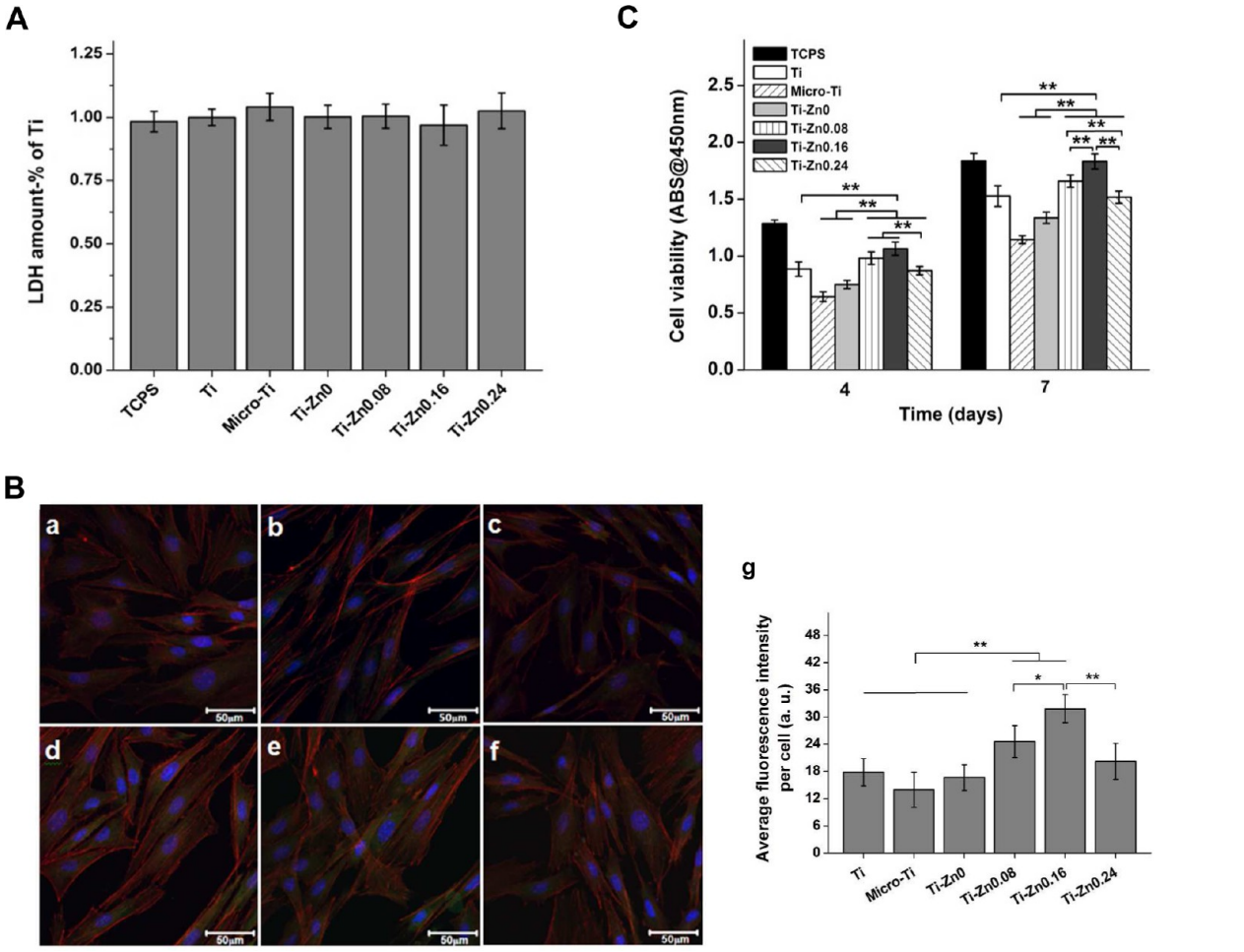

Figure 4. Biocompatibility assays: (A) LDH of osteoblasts cultured on different substrates for 3 d (n = 6); (B) Representative fluorescence images of osteoblasts adhered to (a) Ti, (b) Micro-Ti, (c) Ti−Zn0, (d) Ti−Zn0.08, (e) Ti−Zn0.16, and (f) Ti−Zn0.24; (g) quantitative fluorescence intensity of vinculin from osteoblasts grown onto different substrates (n = 50); (C) Cell viability of osteoblasts adhered to different substrates after culture for 4 and 7 d (n = 6), *p < 0.05, **p < 0.01.

To evaluate the property of hydrophilic/hydrophobic, water contact angles of different substrates were characterized in this study, respectively. As show in Figure 1D, native Ti substrates displayed contact angle of ∼72 ± 4°. Micro-Ti substrates showed hydrophobic wettability with contact angle of 104 ± 5°, which was related to its relatively regular valley-like surface structure.[34,35] However, the sol−gel coated substrates (Ti−Zn0, Ti−Zn0.08, Ti−Zn0.16 and Ti−Zn0.24) displayed moderate wettability with contact angles from 81° to 87°, which was potentially important for cell adhesion.

To reveal the crystalline structures of different substrates, XRD patterns were recorded and shown in Figure 2A. Native titanium displayed characteristic patterns, such as (100), (002), (101), (102), (110), (103), and (112). After acid etching, additional peaks at $2\theta \approx 40.3°$ and 59.5° were observed, which were attributed to TiH_2 (Figure 2A,b). For sol−gel coated samples, it was found that small feature peaks of rutile phase were detected, and no feature peaks of Zn were detected in any samples (Figure 2A,c−f).

To further evaluate the surface elemental composition, the XPS survey spectra of all substrates were measured and presented in Figure 2B. From the spectra of Ti (Figure 2B,a), Micro-Ti (Figure 2B,b) and Ti−ZnO (Figure 2B,c), the feature peaks of Ti and O could be observed. The peak at 459.8 eV was assigned to Ti 2p3 and the peak at 530.1 eV was ascribed to O 1s. These results suggest that Ti was mainly presented as a form of TiO_2 at the outermost surfaces of materials.[36] Besides the peaks of Ti and O, the feature peaks of Zn were detected from the spectra of Zn-incorporated samples (Figure 2B,d−f). It had been identified that the peaks at ∼1045.2 and 1023.1 eV were assigned to Zn 2p1 and Zn 2p3, which belong to ZnO.[37] Meanwhile, the other zinc peaks, such as Zn 2s, Zn 3s, and Zn 3sp1, also belonged to ZnO by referring to the NIST X-ray Photoelectron Spectroscopy Database. Except for the peaks of Ti, O, and Zn, the C signal was also observed mainly due to surface contamination.[38] Quantitative element contents of different Ti substrates are listed in Figure 2B,g. At ∼8.05 atom %, 13.54 atom %, and 19.73 atom % of Zn contents were found from Ti−Zn0.08, Ti−Zn0.16, and Ti−Zn0.24 substrates, respectively.

Previous studies reported that zinc ions with high concentration would cause cytotoxicity.[28,29] Thus, it was necessary to optimize the content of zinc in the Zn−TiO_2 coatings. The release of Zn ions from different Zn-incorporated Micro-Ti substrates was measured via ICP-OES. Approximately 1.08, 1.65, and 2.06 ppm of zinc ions released from Ti−Zn0.08, Ti−Zn0.16, and Ti−Zn0.24 substrates within four weeks, respectively (Figure 2C). Relative to the whole release process,

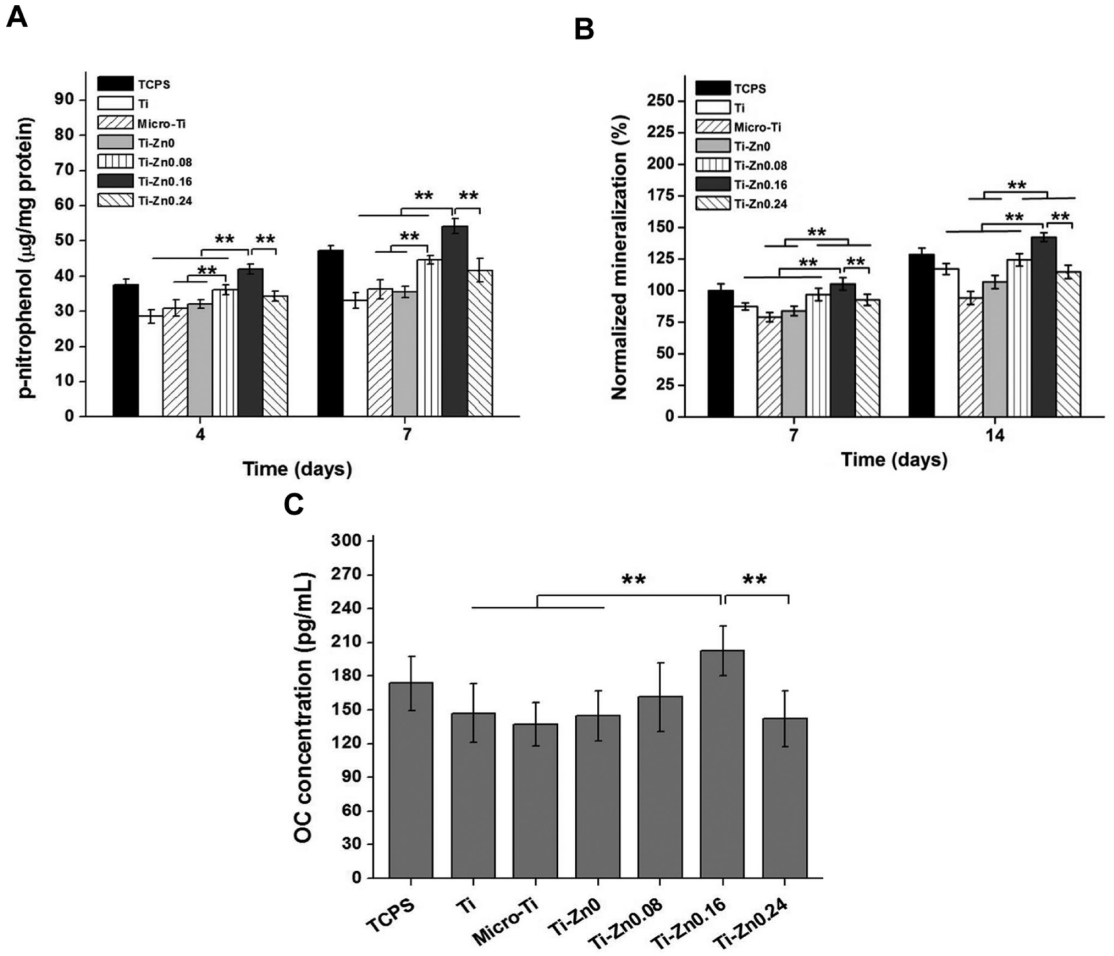

Figure 5. Cellular function assay: (A) Alkaline phosphatase activity of osteoblasts adhered to different Ti substrates after culture for 4 and 7 d, respectively; (B) Mineralization of osteoblasts after culture for 7 and 14 d, respectively; and (C) Osteocalcin production of osteoblasts cultured onto different Ti substrates for 14 d. Error bars represent means ± SD for $n = 6$, $^{**}p < 0.01$.

a quick release of zinc ions occurred at the first week. The concentration of zinc ions reached ~0.62, 0.86, and 1.12 ppm from above corresponding samples. Because of the reduction of zinc ions at the coating layer and deposition of other ions on surface,[39] the release rate of zinc ions slowed after the first week. Previous studies confirmed that maximum concentration of 2 ppm Zn ions was in the safe range without obvious cytotoxicity.[28,40] Thus, we could proceed to further biological assays using the prepared samples.

Second, we evaluated the antibacterial property of the different Ti substrates to both Gram-positive (*Staphylococcus aureus*) and Gram-negative (*Pseudomonas aeruginosa*) bacteria via fluorescent staining and CCK-8 assay. Confocal laser scanning microscopy (CLSM) was first employed to investigate the colony formation of bacteria adhered to different Ti substrates. CLSM images of *S. aureus* (Figure 3A) and *P. aeruginosa* (Figure 3C) revealed that there were no significant difference in cell number between Ti, Micro-Ti, and Ti−Zn0. Compared with Ti, Micro-Ti, and Ti−Zn0 samples, however, fewer cells were found on the surface of Zn-incorporated substrates in an order of Ti−Zn0.24 < Ti−Zn0.16 < Ti−Zn0.08. The results suggest that the Zn-incorporated samples had antibacterial property, which was positively correlated to the zinc concentration in the coating layer.

Following, we quantitatively measured cell viability regarding *S. aureus* (Figure 3B) and *P. aeruginosa* (Figure 3D) grown onto different Ti substrates via CCK-8 method. Compared with Ti, Micro-Ti, and Ti−Zn0 substrates, Zn-incorporated samples displayed efficient antibacterial activities against either *S. aureus* or *P. aeruginosa* in an order of Ti−Zn0.24 > Ti−Zn0.16 > Ti−Zn0.08 at different intervals of time. It was consistent with CLSM observation (Figure 3A,C). Previous studies confirmed that antibacterial mechanism of Zn-related materials was attributed to the high concentration of zinc ions or production of reactive oxygen species (ROS).[41−43] In this study, the highest concentration of zinc ions was only ~2 ppm (Figure 2C). Therefore, the generation of ROS was the most likely antibacterial mechanism.

Third, we investigated the cytocompatibility, proliferation and differentiation of MSCs grown onto different substrates *in vitro*. To determine whether the materials had cytotoxicity, LDH assay was performed in this study. It was known that LDH was a cellular protein. Only low LDH level could be detected from cell medium in normal condition. However, once cell apoptosis caused by materials' cytotoxicity was happened, the extracellular LDH would greatly increase and be easily measured via a LDH kit.[44] In this study, no differences about extracellular LDH were found among all samples (Figure 4A). It suggests no obvious cytotoxicity was observed among all substrates

When cells come into contacting with a biomaterial, cell adhesion is the first cellular cascade,[45] following by cell

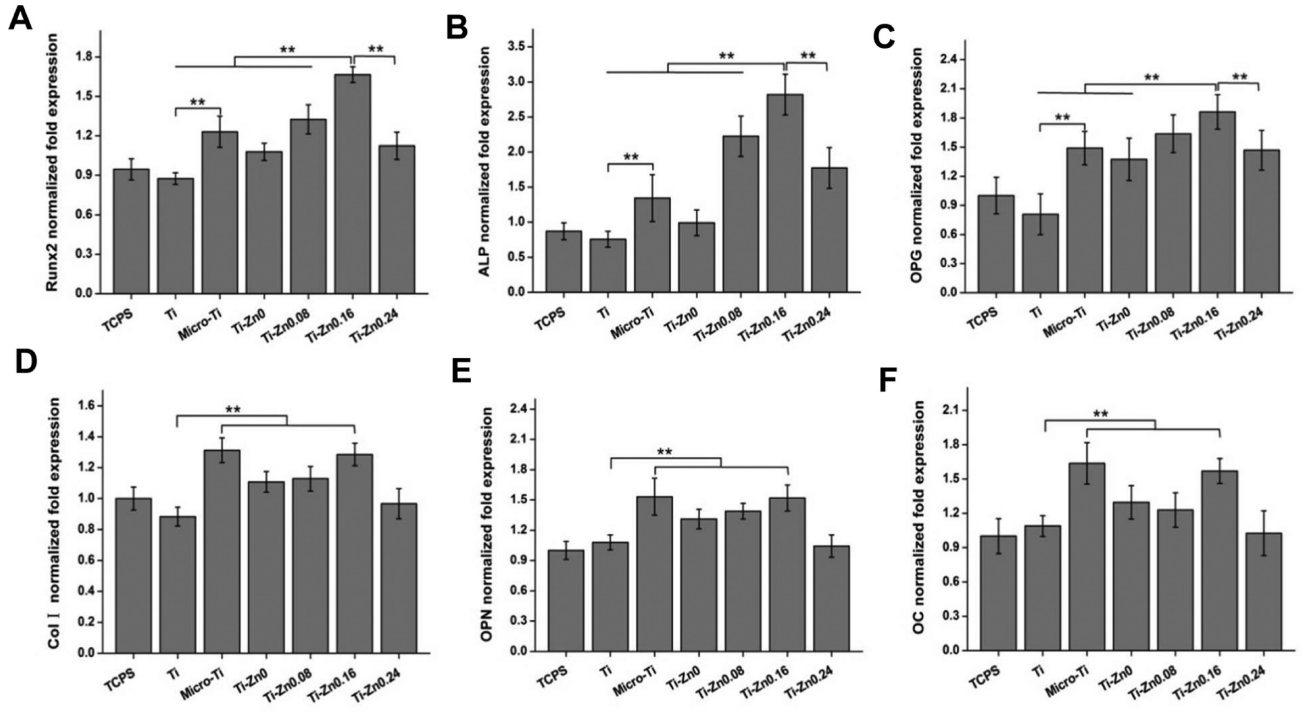

Figure 6. Relative mRNA expression of (A) Runx2, (B) ALP, (C) OPG, (D) Col I, (E) OPN, and (F) OC analyzed by real-time PCR. The value was normalized to β-actin. Error bars represent mean ± SD for $n = 4$, $^{**}p < 0.01$.

proliferation, migration and differentiation, which would be highly regulated by cell adhesion event.[46] It is well-known that surface chemistry, topography, wettability, etc. of a biomaterial would affect cell adhesion. To evaluate cell adhesion behavior, the morphologies of osteoblasts gown onto different Ti substrates were first characterized via CLSM. Discernable differences in morphologies of the osteoblasts adhered on different Ti substrates was observed. Osteoblasts grown on Micro-Ti and Ti−Zn0 substrates spread with small size relative to other substrates (Figure 4B,a−f), which could be attributed to the hydrophobicity of Micro-Ti and the absence of Zn element for Ti−Zn0 substrates, respectively.

Meanwhile, a previous study confirmed that vinculin was a critical cytoplasmic protein for cell focal adhesion, and the higher expression of vinculin could promote higher cell attachment and spreading.[47] Therefore, we then quantified the vinculin expressions of osteoblasts adhered to different Ti substrates (Figure 4B,g). Average fluorescence intensity of vinculin showed that Ti−Zn0.16 and Ti−Zn0.08 were statistically higher ($p < 001$) than those of Ti, Micro-Ti, and Ti−Zn0 substrates. There were no significant difference among Ti, Micro-Ti, and Ti−Zn0 substrates. Ti−Zn0.16 substrates displayed the highest vinculin expression among all groups. The result suggests that Ti−Zn0.16 substrate was beneficial for cell adhesion with appropriate Zn contents.

Moreover, to evaluate the proliferation of osteoblasts cultured onto different substrates, CCK-8 assay was performed (Figure 4C). Osteoblasts adhered to different substrates all proliferated along with time increasing. It could be found that osteoblasts adherent to Micro-Ti and Ti−Zn0 substrates grew not so well as other groups. However, after incorporation of zinc, the Ti−Zn0.08 and Ti−Zn0.16 (rather than Ti−Zn0.24) substrates promoted cell growth, in particular of Ti−Zn0.16 substrates. The viability of osteoblasts grown onto Ti−Zn0.16 substrates was statistically higher ($p < 0.01$) than those of other groups except for tissue culture polystyrene (TCPS) after culture for 4 and 7 d. The result suggests that incorporation of appropriate content of Zn into the surfaces of Micro-Ti would be helpful for osteoblasts proliferation.

To investigate the differentiation of osteoblasts cultured onto different Ti substrates, ALP activity, mineralization and osteocalcin production were measured in this study. ALP and osteocalcin were commonly employed to reflect the osteoblast differentiation at the early and late stage, and mineralization was also used to evaluate the degree of cell differentiation.[8,48] The ALP activity of osteoblasts grown on different substrates is shown in Figure 5A. There was no statistical difference among Ti, Micro-Ti, and Ti−Zn0 substrates. Ti−Zn0.08 and Ti−Zn0.16 substrates displayed significantly higher ($p < 0.01$) ALP activity than those of Ti, Micro-Ti, and Ti−Zn0 substrates after culture for 4 and 7 d. The Ti−Zn0.16 substrates showed the highest ALP activity among all groups, even slightly higher than TCPS; however, no significant difference existed between them.

Next, mineralization was investigated by alizarin red staining after culture for 7 and 14 d (Figure 5B). After culture for 7 d, the mineralization of osteoblasts grown onto Zn-incorporated Ti (Ti−Zn0.08, Ti−Zn0.16, and Ti−Zn0.24) was significantly higher ($p < 0.01$) than those of Micro-Ti and Ti−Zn0 substrates. Ti−Zn0.16 substrates displayed the highest mineralization among all groups. Similar trend was also found after culture for 14 d.

Osteocalcin (OC) was a marker of the late stage of osteoblasts.[48] Thus, we also measured osteocalcin production with an enzyme-linked immunosorbent assay (ELISA) kit after culture for 14 d. Osteoblasts grown on Ti−Zn0.16 substrates displayed significantly higher ($p < 0.01$) osteocalcin production than other groups except for TCPS (Figure 5C). All above results suggest that Ti−Zn0.16 substrates were beneficial for the differentiation of osteoblasts. A previous study confirmed that the released zinc ions from Zn-loaded nanotube arrays

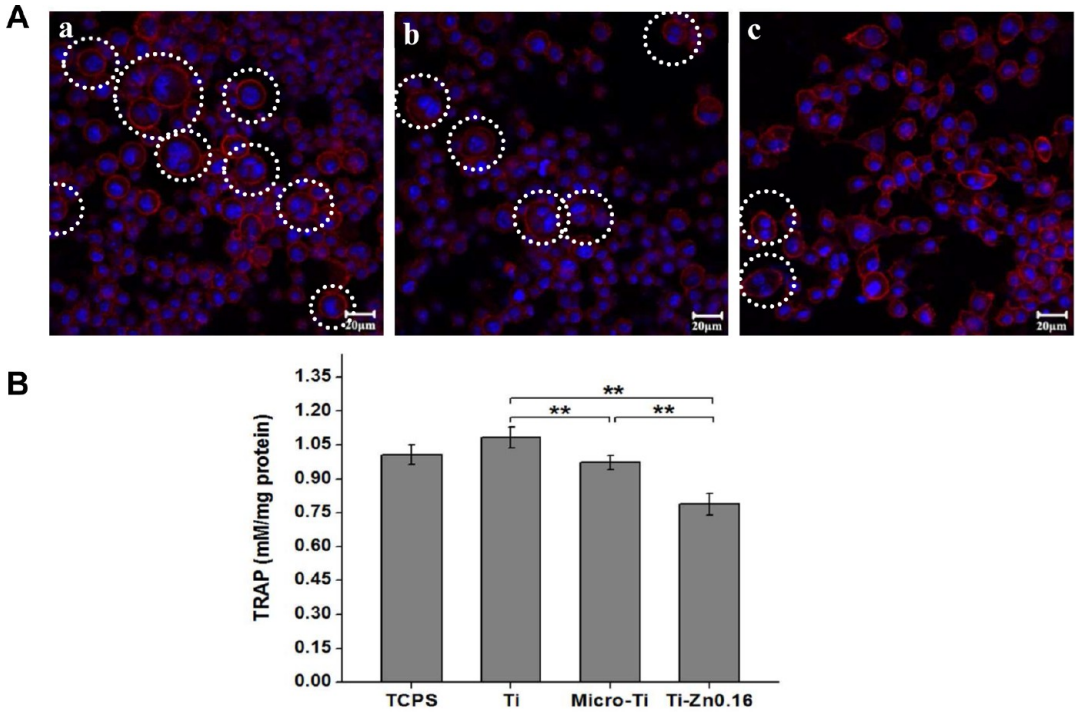

Figure 7. RAW264.7 cells response to different Ti substrates: (A) CLSM images of cells cultured onto (a) Ti, (b) Micro-Ti and (c) Ti−Zn0.16, respectively; and (B) Enzyme activity of TRAP from cells grown onto different Ti substrates (n = 6), $^{**}p < 0.01$.

improved the ERK1/2 signaling which played an important role in cells differentiation.[44] Seo et al. also proved that zinc would lead to a higher production of ALP and collagen to increase bone formation. Thus, we assumed that zinc ions released from the Zn−TiO_2 layer played an important role in the promotion of the differentiation of osteoblasts.[49]

To further evaluate cell differentiation at molecular level, the mRNA expressions of bone formation related genes, including Runt-related transcription factor 2 (Runx2), ALP, osteoprotegerin (OPG), collagen type I (Col I), osteopontin (OPN), and osteocalcin (OC), expressed by osteoblasts grown onto different Ti substrates were measured by real-time PCR (RT-PCR) analysis after culture for 14 d. Previous studies proved that Runx2, a stimulator factor, played an important role in osteogenesis and could regulate the transcription of downstream osteogenic genes, such as ALP, Col I, OC, and OPN.[18,50] Moreover, OPG played an important role in the protection of osteogenesis and inhibition the activity of osteoclast.[51] The result displayed that osteoblasts adhered to Ti−Zn0.16 substrates had the highest Runx2 expression among all groups. Meanwhile, Runx2 was also up-regulated by Micro-Ti substrates comparing with Ti substrates (Figure 6A). It was consistent with previous studies.[12,13] The expressions of ALP and OPG by osteoblasts demonstrated the same trend as Runx2 (Figure 6B,C). Moreover, Col I, OPN, and OC genes had the similar expression trend on different samples (Figure 6D−F). Osteoblasts cultured onto Micro-Ti and Ti−Zn0.16 substrates showed relatively higher Col I, OPN, and OC genes expressions than other groups, nevertheless, no significant difference was observed between them. From the results, we could find that Runx2, ALP, and OPG genes expressions were more sensitive to Zn-incorporated substrates, and Ti−Zn0.16 substrates had the highest genes expression level among all groups (Figure 6A−C). For Col I, OPN, and OC genes, although Ti−Zn0.16 substrates could also up-regulate gene expressions, there were no significant differences between Micro-Ti and Ti−Zn0.16 (Figure 6D−F). Previous studies proved that either microstructure or zinc ions alone could affects the expressions of osteogenic genes.[12,13,52] The different expression tendency of the genes could attribute to the synergistic effects of microstructure and zinc ions. Furthermore, microstructure played a more important role than zinc in the regulation for the expressions of Col I, OPN, and OC genes, whereas the expressions of Runx2, ALP, and OPG genes were dominantly regulated by zinc ions. In short, we could conclude that Ti−Zn0.16 substrates were beneficial for inducing osteogenesis in vitro.

Fourthly, we investigated the antiosteoclast potential of the Zn-incorporated Ti substrates with macrophage cells (RAW264.7) *in vitro*. Bone formation is a dynamic balance between bone formation deriving from osteoblasts differentiation and bone resorption from osteoclasts differentiation.[53] Excessive osteoclasts differentiation leads to osteoporosis. Thus, osteoclasts played an important role in the process of osseointegration.[54] Previous studies confirmed that zinc was a potent inhibitor for osteoclastic maturation.[55,56] Thus, Ti, Micro-Ti, and Ti−Zn0.16 substrates were chosen to evaluate their effects on osteoclast differentiation. In this study, RAW264.7 were cultured on different substrates, because it was reported to be differentiated into osteoclasts with the presence of m-CSF and RANKL.[57] A large number of multinuclear cells (osteoclasts, dash circles) were easily found on Ti and Micro-Ti substrates in comparison with few cells on Ti−Zn0.16 substrates (Figure 7A,a,b vs c). Quantitative tartrate-resistant acid phosphatase (TRAP) activity analysis of RAW264.7 was also performed. The result showed that TRAP activity of RAW264.7 cells grown onto Ti−Zn0.16 substrates was significantly lower ($p < 0.01$) than those of Micro-Ti and Ti substrates, in an order of Ti−Zn0.16 < Micro-Ti < Ti (Figure7B). The result suggests that Ti−Zn0.16 substrates had

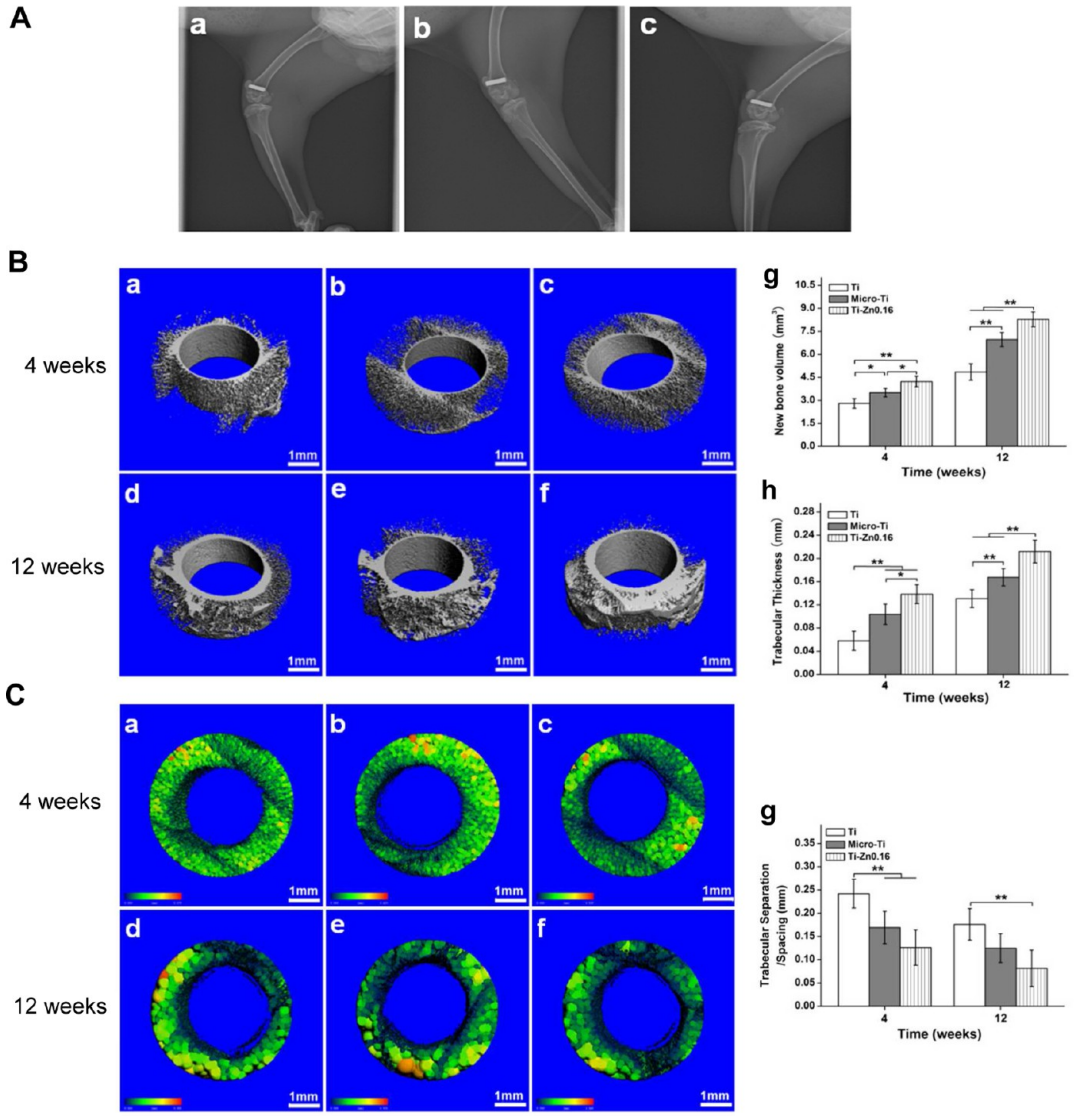

Figure 8. X-ray observation and Micro-CT assay: (A) X-ray photographs of (a) Ti, (b) Micro-Ti and (c) Ti−Zn0.16 after implantation for 4 weeks; (B) New bone formation around different implants: (a, d) Ti, (b, e) Micro-Ti, and (c, f) Ti−Zn0.16 after implantation for 4 weeks (a−c) and 12 weeks (d−f); quantitative analysis of new bone volume (g) and trabecular thickness (h); and (C) Trabecular separation with different implants of (a, d) Ti, (b, e) Micro-Ti, and (c, f) Ti−Zn0.16 after implantation for 4 weeks (a−c) and 12 weeks (d−f); quantitative analysis of trabecular separation (g). Error bars represent mean ± SD for $n = 4$, $^{*}p < 0.05$, $^{**}p < 0.01$.

a great potential for inhibiting the differentiation of RAW264.7 cells. It implies that Ti−Zn0.16 materials could be employed for the fabrication of functional orthopedic implants for patients suffering from osteoporosis.

Finally, we further investigated the osteogenesis of the screened substrates *in vivo*. To evaluate the locations of implants and/or inflammatory reactions after implantation, we took X-ray radiographs after implantation for four weeks (Figure 8A). The images showed that Ti, Micro-Ti, and Ti−Zn0.16 implants were located well at the surgery sites. No dislocation or loosening was observed with all implants. Meanwhile, no obvious inflammatory reactions or adverse effects around the implants were observed.

To investigate osseointegration of different Ti implants, Micro-CT analysis was performed. The new bone volume (BV), trabecular thickness (TH) and trabecular separation/spacing (SP) were referred to new bone formation. From the three-dimensional images of new bone surrounding different implants after implantation for 4 and 12 weeks (Figure 8B,a−f), it could be found that there were more new bone (gray/white parts) around Ti−Zn0.16 implants than other groups in an order of Ti−Zn0.16 > Micro-Ti > Ti. The new bone formation around all implants gradually increased from 4 weeks to 12 weeks (Figure 8B,d−f vs a−c). Quantitative analysis of new bone (NB) and TH showed that those around Ti−Zn0.16 implants were significantly higher ($p < 0.05$ or $p < 0.01$) than Micro-Ti and Ti implants (Figure 8B,g,h). Moreover, better bone formation around Micro-Ti implants than that of Ti implants was also observed.

Furthermore, we measured the trabecular separation/spacing (SP) between implants and nature bone with three-dimensional simulation (Figure 8C,a−f) and quantitative analysis (Figure 8C,g). In the three-dimensional simulation, various colors were used to refer the trabecular separation. The colors from black to red represent trabecular separation changing from small to large. The SP of Ti−Zn0.16 was the lowest among all groups

and significantly lower ($p < 0.01$) than that of Ti implants (Figure 8C,g). All above results indicate that Ti−Zn0.16 implants were superior to Ti and Micro-Ti implants for inducing the formation of new bone.

To evaluate the interfacial strength of different implants at the interface between implants and native bone, push-out test was performed after implantation for 4 and 12 weeks in this study (Figure 9). After implantation for four weeks, the

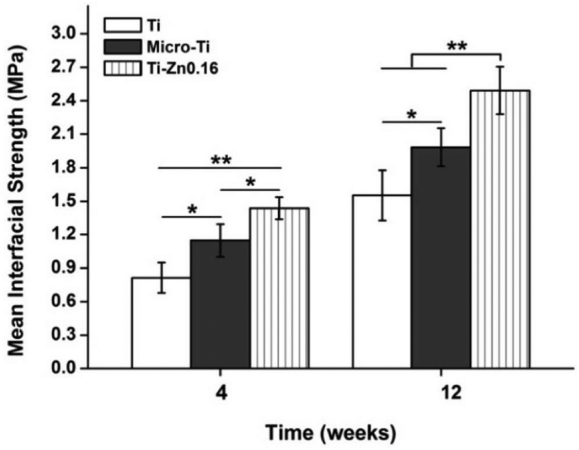

Figure 9. Push-out strength of different implants after implantation for 4 and 12 weeks, respectively. Error bars represent mean ± SD for n = 4, *$p < 0.05$, **$p < 0.01$.

interfacial strength of Ti−Zn0.16 implants was significantly higher ($p < 0.05$ and $p < 0.01$) than those of Micro-Ti and Ti implants, respectively. After implantation for 12 weeks, the interfacial strength of Ti−Zn0.16 implants was statistically higher ($p < 0.01$) than those of Micro-Ti and Ti implants, respectively. Meanwhile, Micro-Ti implants displayed higher ($p < 0.05$) interfacial strength than that of Ti implants after implantation for either 4 weeks or 12 weeks.

To investigate osteogenesis at the bone-implant interface, hematoxylin and eosin (H&E) and Masson's trichrome (MT) staining were employed for decalcified samples, respectively. A little loose osteoid tissue was found at the interfaces of Ti-bone and Micro-Ti-bone, whereas relatively compact osteoid tissue was observed at the interface of Ti−Zn0.16-bone after implantation for four weeks (Figure 10A,a−c, arrows). After implantation for 12 weeks, all osteoid tissues around different Ti implants increased when comparing with those after implantation for 4 weeks (Figure 10A,d−f vs a−c, arrows). It could be found that there was no gap between new bone and native bone surrounding the Ti−Zn0.16 implants (Figure 10A,f, arrows).

Next, to further evaluate the mature degree of newly formed bone, Masson's trichrome (MT) staining was employed. With MT staining, the matured bone was revealed as red color while newly formed bone was presented as blue color. There were much newly formed bone (blue) around Ti−Zn0.16 implant, which was slightly higher than those of Ti and Micro-Ti implants after implantation for 4 weeks (Figure 10B,c vs a,b, arrows). After implantation for 12 weeks, similar trend was also observed. More importantly, the new bone formed at the interface of Ti−Zn0.16-bone became to be mature (Figure10B,f, arrows).

Generally, Zinc was used as one kind of additive element in the preparation of biomaterials for promoting osteogenesis.[58]

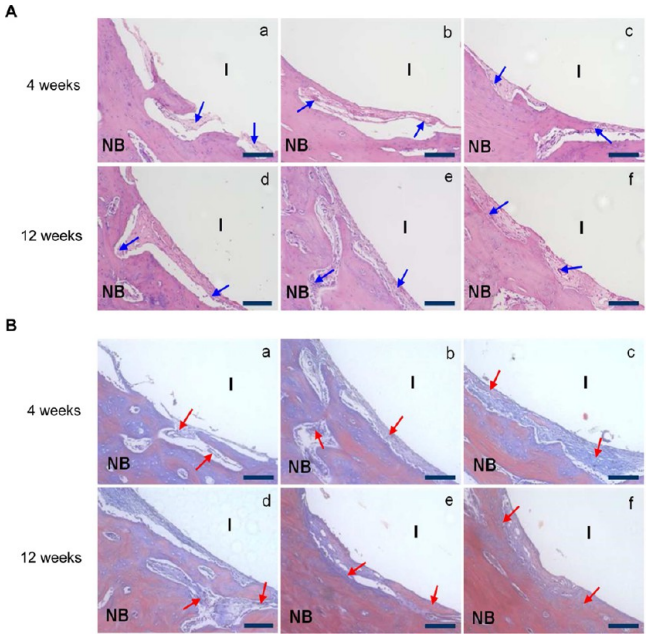

Figure 10. Histological observations: (A) H&E staining images of different implantations: (a, d) Ti, (b, e) Micro-Ti, and (c, f) Ti−Zn0.16 after implantation for 4 weeks (a−c) and 12 weeks (d−f), respectively. I: implant; NB: natural bone. The arrows refer to the newly formed bone; and (B) Masson's trichrome staining images of different implantations: (a, d) Ti, (b, e) Micro-Ti, and (c, f) Ti−Zn0.16 after implantation for 4 weeks (a, b, c) and 12 weeks (d, e, f), respectively. The arrows represent the formed bone trabeculae (TB). Scale bar: 150 μm.

Nevertheless, an appropriate content of zinc was critically important for the biological functions of cells. Previous studies verified that high concentrations of zinc ions even led to cytotoxicity.[28,29] In this study, the content of zinc for the fabrication of Zn-incorporated samples were optimized and confirmed that Ti−Zn0.16 (13.5 at%) substrate was the optimal one, which was proved by cells experiments (osteoblasts/osteoclasts) in vitro. Moreover, in vivo results also confirmed that Ti−Zn0.16 could efficiently induce new bone formation. The preliminary mechanism is proposed as follows: first, the sustained release of zinc ions promoted the proliferation of osteoblasts,[20] up-regulated the genes expressions of Runx2, ALP and OPG,[52] as well as inhibited the osteoclast differentiation;[56] second, microstructure contributed to the expressions of Col I, OPN and OC genes. Both factors synergistically promoted the osseointegration of Ti−Zn0.16 implants for bone formation. More detailed molecular mechanism should be investigated by using signal blocking techniques in the future.

CONCLUSION

In summary, we fabricated Zn-incorporated coatings with optimal zinc contents onto the surface of micro-Ti via a sol−gel process with assistance of spin-coat technique, which demonstrated great potential for improving osteoblasts proliferation/differentiation from cellular and molecular levels, inhibiting bacteria adhesion and osteoclasts differentiation *in vitro*, as well as osseointegration *in vivo*. The potential mechanism was proposed that both microstructure and zinc ions contributed to the improved osseointegration of Ti−Zn0.16 implant. This study provides an alternative for the

biofunctionalization of titanium-based implants for orthopedic applications.

EXPERIMENTAL SECTION

Materials. Native titanium (Ti) disks (diameter: 15 mm; thickness: 3 mm) and rods (diameter: 3 mm; length: 13 mm) were provided by Northwest Institute for Nonferrous Metal Research, China. Cell counting kit-8 (CCK-8) kit, lactate dehydrogenase (LDH) assay kit, *p*-nitrophenyl phosphate, and bicinchoninic acid (BCA) assay kit were obtained from Beyotime Biotechnology Co. (Jiangsu, China). Osteocalcin assay kit was provided by Uscnlife Science and Technology Co., Ltd. (Wuhan, China). Mouse recombinant receptor activator of nuclear factor κ-B ligand (RANKL) and macrophage colony-stimulating factor (m-CSF) were purchased from PeproTech, Inc. (NJ, USA). Rhodamine−phalloidin was bought from Invitrogen Co. (USA). Hoechst 33258 was provided by Sigma-Aldrich Co. (St. Louis, MO, USA). Antivinculin antibody was purchased from Santa Cruz Biotechnology Co. (USA). Mouse antigoat fluorescein isothiocyanate (FITC)-conjugated secondary antibody was supplied by ZSGB-BIO Co. (China). Other chemicals were purchased from Oriental Chemical Co. (Chongqing, China).

Sample Preparation. Ti disks were first polished with diamond pastes (No. 600−2000) and then ultrasonically cleaned with ethanol, acetone, ethanol, and distilled water, each for 15 min. After drying, the disks were etched with 0.5% hydrofluoric acid (HF) at 80 °C for 30 min to obtain the microrough titanium (Micro-Ti). The Micro-Ti substrates were then rinsed with distilled water, and $ZnCl_2$ solutions with different concentrations (0, 0.08, 0.16, and 0.24 M) in EtOH/0.1 M tetrabutyl titanate were spin-coated (3000 rpm for 45 s) on the surface of Micro-Ti substrates. Finally, the coated disks were calcined at 450 °C for 2 h with a heating rate of 5 °C/min and then naturally cooled to ambient temperature. The coated samples were denoted as Ti−Zn0, Ti−Zn0.08, Ti−Zn0.16, and Ti−Zn0.24, respectively.

Sample Characterization. Surface morphologies of different Ti substrates were characterized by field emission scanning electron microscopy (SEM) (FEI Nova 400 Nano SEM, Phillips Co, Holland). The crystalline phases of samples were characterized by X-ray diffraction (D/Max 2500PC, Rigaku, Japan). The surface chemistry of the different Ti substrates was determined by X-ray Photoelectron Spectroscopy (XPS) (Model PHI 5400, PerkinElmer, USA). The surface roughness (Rq) of different samples was measured by a surface profiler (Veeco Dektak 150, USA), and water contact angle measurements were performed with a video-based optical system (Model 200, Future Scientific, Taiwan, China). Each water drop (5 μL) was deposited to the sample surface and kept for 15 s at ambient temperature.[33] Then, an image of the drop was recorded by a camera and analyzed with the software supplied by the manufacturer. All measurements were conducted at room temperature.

Zn Ion Release. Ti−Zn0 and Zn-incorporated samples (Ti−Zn0.08, Ti−Zn0.16, and Ti−Zn0.24) were immersed in 5 mL simulated body fluid (SBF) solution and kept in an incubator at 37 °C for 1, 4, 7, 14, 21, and 28 d. The concentrations of released zinc ions at different intervals of time were measured by an inductively coupled plasma/optical emission spectroscopy (ICP-OES; Vista AX, Varian, USA).

Bacteria Culture. Both *S. aureus* and *P. aeruginosa* were purchased from ATCC. The bacteria were cultured in Mueller−Hinton Broth (MHB) medium with shaking (150 rpm) at 37 °C. Then, the bacteria were used in the following experiments.

Bacteria Viability. Bacteria of *S. aureus* and *P. aeruginosa* were cultured onto Ti, Micro-Ti, Ti−Zn0, Ti−Zn0.08, Ti−Zn0.16, Ti−Zn0.24, and tissue culture polystyrene (TCPS) at an initial density of 1×10^6 cells/cm^2 for 12, 24, and 48 h, respectively. After rinsing with phosphate buffered saline (PBS) three times, 200 μL of fresh MHB medium and 20 μL of CCK-8 solution were added and incubated at 37 °C for another 1 h. The optical density of the solution was determined with a spectrophotometric microplate reader (Bio-Rad 680, USA) at a wavelength of 450 nm. In addition, the colony formation of both *S. aureus* and *P. aeruginosa* onto different substrates was observed by confocal laser scanning microscopy (CLSM, TCS SP5, Leica, Germany) after culture at 37 °C for 24 h.

Cell Culture. Osteoblasts were isolated from neonatal rat calvaria and RAW264.7 cells (osteoclast-like cells) were provided by the Third Military Medicine University (Chongqing, China). Both osteoblasts and RAW264.7 cells were cultured in DMEM (with high glucose) supplemented with 10% fetal bovine serum (FBS) at 37 °C under 5% CO_2 atmosphere. Cell culture media was initially changed at the first day and every 2 d thereafter. Osteoblasts at the third passage were used for the following experiments.

Lactate Dehydrogenase Activity Assay. Lactate dehydrogenase (LDH) was a marker to cytotoxicity of materials. Osteoblasts were seeded onto different Ti substrates at a density of 1×10^4 cells/cm^2. After it was cultured for 3 d, the culture media were collected and then centrifuged to obtain the supernatant for measuring LDH activity. The activity was measured with an LDH assay kit. The absorbance of the solution was measured with a spectrophotometric microplate reader (Bio-Rad 680, USA) at a wavelength of 490 nm.

Cell Morphology. Osteoblasts were cultured onto different substrates at an initial density of 4×10^3 cells/cm^2 in a 24-well plate for 48 h. Then, cells were fixed with 4% paraformaldehyde at 4 °C for 30 min and permeabilized with 0.2% Triton X-100 for another 2 min. After rinsing with PBS three times, nonspecific binding sites were blocked with 10% bovine serum albumin (BSA) for 30 min. Next, 200 μL of primary antibody against vinculin (1:200) was added to each well and kept at 4 °C overnight. Next, after rinsing with PBS three times, 200 μL of second antibody (1:400) was added and kept at ambient temperature for another 1 h. Subsequently, samples were stained with rhodamine-phalloidin at 4 °C overnight and counter stained with Hoechst 33258 for 5 min, respectively. Finally, the stained samples were mounted with 90% glycerinum and observed with CLSM (TCS SP5, Leica, Germany).

Proliferation Assay. CCK-8 assay was used to evaluate proliferation of osteoblasts cultured on different substrates (n = 6). Osteoblasts were seeded onto different Ti substrates at a density of 1×10^4 cells/cm^2. After culture for 4 and 7 d, 200 μL of new medium and 20 μL of CCK-8 solution were added to each well of a 24-well plate and then incubated for another 1.5 h. Finally, the incubated solution was measured was measured with a spectrophotometric microplate reader (Bio-Rad 680, USA) at a wavelength of 450 nm.

Alkaline Phosphatase (ALP) Activity. The ALP assay was performed according to a previous study.[59] Osteoblasts were seeded onto different Ti substrates at a density of 1×10^4 cells/cm^2. After culture for 4 and 7 d, osteoblasts were lysed by 1% Triton X-100 with three freeze−thaw cycles. Following

Table 1. Real-Time Polymerase Chain Reaction Primers Used in This Study

target gene	gene bank (accession no.)	primers	product size (bp)
β-actin	NM_031144.2	GGAGATTACTGCCCTGGCTCCTA	150
		GACTCATCGTACTCCTGCTTGCTG	
Runx2	NM_053470.2	GCCGTAGAGAGCAGGGAAGAC	150
		CTGGCTTGGATTAGGGAGTCAC	
ALP	NM_013059	AGCGACACGGACAAGAAGC	183
		GGCAAAGACCGCCACATC	
Col I	NM_053304.1	CCTGAGCCAGCAGATTGA	106
		TCCGCTCTTCCAGTCAG	
OPN	M99252	GACAGCAACGGGAAGACC	216
		CAGGCTGGCTTTGGAACT	
OC	M11777	GAGGGCAGTAAGGTGGTGAA	154
		CGTCCTGGAAGCCAATGTG	
OPG	RNU94330	GCCCAGACGAGATTGAGAG	173
		CAGACTGTGGGTGACGGTT	

centrifugation the lysate, the total intracellular protein and ALP activity were determined from the supernatant, respectively. In this study, *p*-nitrophenyl phosphate and bicinchoninic acid (BCA) assay kit were used to measure the total intracellular protein content and ALP activity. The solution absorbance regarding ALP and total intracellular protein content were measured with a spectrophotometric microplate reader (Bio-Rad 680, USA) at wavelengths of 490 and 570 nm, respectively.

Osteocalcin Assay. Osteoblasts were seeded onto different Ti substrates at a density of 1×10^4 cells/cm^2. The osteocalcin production was measured with an enzyme-linked immunosorbent assay (ELISA) after culture osteoblasts for 14 d. Briefly, 1 mL of culture medium was collected and reacted with antiosteocalcin monoclonal antibody and horseradish peroxidase (HRP)-conjugated antibody. Tetramethylbenzidine (TMB) was used as chromogenic substrate. The reaction was quenched with hydrochloric acid. Then the absorbance of the mixture solution was measured with a spectrophotometric microplate reader at a wavelength of 450 nm.

Quantification of Mineralization. Osteoblasts were seeded onto different Ti substrates at a density of 1×10^4 cells/cm^2. After culture for 7 and 14 d, osteoblasts grown onto different substrates were stained by alizarin red S according to a previous study.[57] Briefly, cells were fixed with 4% paraformaldehyde at 4 °C for 30 min and stained with alizarin red S (40 mM, pH 4.1) at ambient temperature for another 20 min. After washing with distilled water three times, acetic acid (10% v/v) solution was added to each well and incubated at 37 °C for 30 min. Subsequently, cells were scraped from the sample surface and transferred to a vial and vortexed for 30 s. After it was heated at 85 °C for 10 min and centrifuged for 15 min, the supernatant was transferred to a new vial, and 10% ammonium hydroxide was added to neutralize the acid. The absorbance of the solution was measured with a microplate reader (Bio-Rad 680, USA) at a wavelength of 405 nm.

Real-Time Polymerase Chain Reaction. Osteoblasts were seeded onto different Ti substrates at a density of 1×10^4 cells/cm^2. After culture for 14 d, the total RNA was extracted according to the instruction of RNA extract kit (Bioteck Co.). Then, the extracted RNA was reversely transcribed for the first strand cDNA synthesis. Real-time PCR was performed with Bio-Rad CFX Manager system. Amplification was performed with two-step cycling conditions at 98 °C for 3 min, followed by 40 cycles at 98 °C for 2 s, 58 °C for 10 min.[48] The primers are listed in Table 1, and the targeted gene expression was normalized to β-actin.

Osteoclasts Differentiation. RAW264.7 cells were seeded onto different Ti substrates at a density of 3×10^4 cells/cm^2 and cultured with the differentiation media containing 10% FBS, 50 ng/mL receptor activator of nuclear factor κ-B ligand (RANKL) and 20 ng/mL macrophage colony-stimulating (m-CSF). After culture for 7 d, the cytoskeleton and nuclei of osteoclast-like cells were stained with rhodamine−phalloidin and Hoechst 33258 as above-mentioned. The cell morphology was observed with CLSM (TCS SP5, Leica, Germany).

After culture for 7 d, the tartrate-resistant acid phosphatase (TRAP) activity of RAW264.7 cells was measured.[48] Briefly, cells were lysed with 0.1% Triton X-100 buffer containing 80 mM sodium tartrate and 90 mM citrate (pH 4.8) for 10 min. Then, the *p*-nitrophenyl phosphate substrate solution was added and incubated 37 °C for 5 min. The reaction was stopped with 0.5 M NaOH. The optical density of the mixed solution was measured with a microplate reader (Bio-Rad 680, USA) at a wavelength of 405 nm.

Implantation Surgery. The in vivo experiments were conducted according to the guidelines of the Institutional Animal Care and Use Committee of China. 60 mature New Zealand white rabbits with average weight of ∼2.5−3 kg were used in this study. The Ti, Micro-Ti, and Ti−Zn0.16 implants were implanted into the epiphysis of femur. The operation process was performed as a previous report.[48] The rabbits were anesthetized by intravenous injection of 2% pentobarbital sodium. The operation areas were shaved and sterilized, and an incision of ∼3 cm was made to expose the femoral epiphysis. Then, a cylindrical hole (3.0 mm in diameter) with length more than 13 mm was created using a surgical drill, and different rods were implanted into the holes. Finally, the skin and soft tissue layers were sutured with the absorbable sutures.

X-ray Observation and Micro-CT Assay. After implantation for four weeks, X-ray radiographs were taken to reveal the conditions of the implants. After implantation for 4 and 12 weeks, the rabbits were sacrificed via intravenous injection of air. The femora epiphyses containing implants were collected and fixed immediately with 10% formalin. The samples were scanned with Micro-CT (SCANCO Medical AG, Viva CT40) to measure the new bone formations at the range of 1 mm surrounding implants.

Push-out Test. The push-out test was performed using a universal material testing system (Instron, High Wycombe,

U.K.). The tests were performed at the rate of 5 mm/min.[60] The failure load was defined as the maximum push strength. The ultimate interfacial strength (δ) was calculated according the equation[61] $\delta = P/\pi dh$; where P was the push-out load (N), d (mm) was the diameter of the rods, and h (mm) was the length of the rods.

Histological Analysis. After implantation for 4 and 12 weeks, all femoral epiphysis containing implants were collected and immediately fixed with 10% formalin at 4 °C for 48 h. Then, the samples were decalcified with 12% ethylene diamine tetraacetic acid (EDTA) for 21 d. The EDTA solution was changed every 3 d. After decalcification treatment, all Ti implants were taken out carefully without destroying bone tissue surrounding implants. Next, samples were dehydrated in graduated ethanol solutions and then embedded with paraffin. Finally, the decalcified sections were stained with hematoxylin and eosin (H&E) and Masson's trichrome (MT). The images of the slices were taken with an inverted microscope (Olympus, Japan).

Statistical Analysis. All data were expressed as means ± standard deviation (SD). The statistical analysis was performed with OriginPro (version 7.5) via Students's t test and one-way analysis of variance (ANOVA). The confidence levels were set as 95% and 99%.

AUTHOR INFORMATION

Corresponding Author

*E-mail: kaiyong_cai@cqu.edu.cn.

Author Contributions

The manuscript was written through contributions of all authors. All authors have given approval to the final version of the manuscript.

Notes

The authors declare no competing financial interest.

ACKNOWLEDGMENTS

We gratefully acknowledge the financial support from Natural Science Foundation of Chongqing Municipal Government (CSTC, 2011JJJQ10004), Natural Science Foundation of China (51173216 and 31200712), National Key Technology R&D Program of the Ministry of Science and Technology (2012BAI18B04), and Fundamental Research Funds for the Central Universities (CQDXWL-2013-Z002).

REFERENCES

(1) Liu, X.; Chu, P. K.; Ding, C. Surface Modification of Titanium, Titanium Alloys, and Related Materials for Biomedical Applications. *Mater. Sci. Eng., R.* **2004**, *92*, 49−121.

(2) Gil, F. J.; Manzanares, N.; Badet, A.; Aparicio, C.; Ginebra, M. P. Biomimetic Treatment on Dental Implants for Short-Term Bone Regeneration. *Clin. Oral Invest.* **2014**, *18*, 59−66.

(3) Tschernitschek, H.; Borchers, L.; Geurtsen, W. Nonalloyed Titanium as a Bioinert Metal—A Review. *Quintessence Int.* **2005**, *36*, 523−530.

(4) Cai, K.; Hou, Y.; Hu, Y.; Zhao, L.; Luo, Z.; Shi, Y.; Lai, M.; Yang, W.; Liu, P. Correlation of the Cytotoxicity of TiO2 Nanoparticles with Different Particle Sizes on a Sub-200-nm. *Small* **2011**, *7*, 3026−3031.

(5) Hetrick, E. M.; Schoenfisch, M. H. Reducing Implant-Related Infections: Active Release Strategies. *Chem. Soc. Rev.* **2006**, *35*, 780−789.

(6) Zhao, B.; van der Mei, H. C.; Subbiahdoss, G.; de Vries, J.; Rustema-Abbing, M.; Kuijer, R.; Busscher, H. J.; Ren, Y. Soft Tissue Integration Versus Early Biofilm Formation on Different Dental Implant Materials. *Dent. Mater.* **2014**, *30*, 716−727.

(7) Yuan, K.; Chan, Y. J.; Kung, K. C.; Lee, T. M. Comparison of Osseointegration on Various Implant Surfaces after Bacterial Contamination and Cleaning: A Rabbit Study. *Int. J. Oral Maxillofac. Implants* **2014**, *29*, 32−40.

(8) Lai, M.; Cai, K.; Zhao, L.; Chen, X.; Hou, Y.; Yang, Z. Surface Funtionalization of TiO_2 Nanotubes with Bone Morphogenetic Protein 2 and Synergistic Effect on the Differentiation of Mesenchymal Stem Cells. *Biomacromolecules* **2011**, *12*, 1097−1105.

(9) Yada, M.; Inoue, Y.; Sakamoto, A.; Torikai, T.; Watari, T. Synthesis and Controllable Wettability of Micro- and Nanostructured Titanium Phosphate Thin Films Formed on Titanium Plates. *ACS Appl. Mater. Interfaces* **2014**, *6*, 7695−7704.

(10) Cai, K.; Hu, Y.; Luo, Z.; Kong, T.; Lai, M.; Sui, X.; Wang, Y.; Yang, L.; Deng, L. Cell-Specific Gene Transfection from a Gene-Functionalized Poly(D,L-lactic acid) Substrate Fabricated by the Layer-by-Layer Assembly Technique. *Angew. Chem., Int. Ed.* **2008**, *47*, 7479−7481.

(11) Yavari, S. A.; van der Stok, J.; Chai, Y. C.; Wauthle, R.; Birgani, Z. T.; Habibovic, P.; Mulier, M.; Schrooten, J.; Weinans, H.; Zadpoor, A. A. Bone Regeneration Performance of Surface-Treated Porous Titanium. *Biomaterials* **2014**, *35*, 6172−6181.

(12) Olivares-Navarrete, R.; Hyzy, S. L.; Hutton, D. L.; Erdman, C. P.; Wieland, M.; Boyan, B. D.; Schwartz, Z. Direct and Indirect Effects of Microstructured Titanium Substrates on the Induction of Mesenchymal Stem Cell Differentiation Towards the Osteoblast Lineage. *Biomaterials* **2010**, *31*, 2728−2735.

(13) Schwartz, Z.; Olivares-Navarrete, R.; Wieland, M.; Hutton, D. L.; Boyan, B. D. Mechanisms Regulating Increased Production of Osteoprotegerin by Osteoblasts Cultured on Microstructured Titanium Surfaces. *Biomaterials* **2009**, *30*, 3390−3396.

(14) Conserva, E.; Menini, M.; Ravera, G.; Pera, P. The Role of Surface Implant Treatments on the Biological Behavior of SaOS-2 Osteoblast-like Cells. An in Vitro Comparative Study. *Clin. Oral Implants Res.* **2013**, *24*, 880−889.

(15) Li, Y.; Gao, Y.; Shao, B.; Xiao, J.; Hu, K.; Kong, L. Effects of Hydrofluoric Acid and Anodised Micro and Micro/Nano Surface Implants on Early Osseointegration in Rats. *Br. J. Oral Maxillofac. Surg.* **2012**, *50*, 779−783.

(16) Zhao, L.; Mei, S.; Chu, P. K.; Zhang, Y.; Wu, Z. The Influence of Hierarchical Hybrid Micro/Nano-Textured Titanium Surface with Titania Nanotubes on Osteoblast Functions. *Biomaterials* **2010**, *31*, 5072−5082.

(17) Hu, Y.; Cai, K.; Zhang, R.; Luo, Z.; Yang, L.; Jandt, K. D. Surface Mediated in Situ Differentiation of Mesenchymal Stem Cells on Gene-Functionalized Titanium Films Fabricated by Layer-by-Layer Technique. *Biomaterials* **2009**, *30*, 3626−3635.

(18) Ma, X. Y.; Feng, Y. F.; Ma, Z. S.; Li, X.; Wang, J.; Wang, L.; Lei, W. The Promotion of Osteointegration under Diabetic Conditions Using Chitosan/Hydroxyapatite Composite Coating on Porous Titanium Surfaces. *Biomaterials* **2014**, *35*, 7259−7270.

(19) Schliephake, H.; Bötel, C.; Förster, A.; Schwenzer, B.; Reichert, J.; Scharnweber, D. Effect of Oligonucleotide Mediated Immobilization of Bone Morphogenic Proteins on Titanium Surfaces. *Biomaterials* **2012**, *33*, 1315−1322.

(20) Qiao, Y.; Zhang, W.; Tian, P.; Meng, F.; Zhu, H.; Jiang, X.; Liu, X.; Chu, P. K. Stimulation of Bone Growth Following Zinc Incorporation into Biomaterials. *Biomaterials* **2014**, *35*, 6882−6897.

(21) Bagherifardet, S.; Ghelichi, R.; Khademhosseini, A.; Guagliano, M. Cell Response to Nanocrystallized Metallic Substrates Obtained through Severe Plastic Deformation. *ACS Appl. Mater. Interfaces* **2014**, *6*, 7963−7985.

(22) Misra, R. D.; Thein-Han, W. W.; Pesacreta, T. C.; Hasenstein, K. H.; Somani, M. C.; Karjalainen, L. P. Cellular Response of Preosteoblasts to Nanograined/Ultrafine-Grained Structures. *Acta. Biomater.* **2009**, *5*, 1455−1467.

(23) Esteban-Tejeda, L.; Díaz, L. A.; Prado, C.; Cabal, B.; Torrecillas, R.; Moya, J. S. Calcium and Zinc Containing Bactericidal Glass Coatings for Biomedical Metallic Substrates. *Int. J. Mol. Sci.* **2014**, *15*, 13030−13044.

(24) Hu, H.; Zhang, W.; Qiao, Y.; Jiang, X.; Liu, X.; Ding, C. Antibacterial Activity and Increased Bone Marrow Stem Cell Functions of Zn-incorporated TiO_2 Coatings on Titanium. *Acta. Biomater.* **2012**, *8*, 904−915.
(25) Jain, A.; Bhargava, R.; Poddar, P. Probing Interaction of Gram-Positive and Gram-Negative Bacterial Cells with ZnO Nanorods. *Mater. Sci. Eng., C* **2013**, *33*, 1247−1253.
(26) Xu, J.; Ding, G.; Li, J.; Yang, S.; Fang, B.; Sun, H.; Zhou, Y. Zinc-Ion Implanted and Deposited Titanium Surfaces Reduce Adhesion of Streptococccus Mutans. *Appl. Surf. Sci.* **2010**, *256*, 7540−7544.
(27) Berg, J. M.; Shi, Y. The Galvanization of Biology: A Growing Appreciation for the Roles of Zinc. *Science* **1996**, *271*, 1081−1085.
(28) Wätjen, W.; Haase, H.; Biagioli, M.; Beyersmann, D. Induction of Apoptosis in Mammalian Cells by Cadmium and Zinc. *Environ. Health Perspect.* **2002**, *110*, 865−867.
(29) Brauer, D. S.; Gentleman, E.; Farrar, D. F.; Stevens, M. M.; Hill, R. G. Benefits and Drawbacks of Zinc in Glass Ionomer Bone Cements. *Biomed. Mater.* **2011**, *6*, 045007.
(30) Carbajal, L.; Serena, S.; Caballero, A.; Stevens, M. M.; Hill, R. G. Role of ZnO Additions on the Beta/Alpha Phase Relation in TCP Based Materials: Phase Stability, Properties, Dissolution and Biological Response. *J. Eur. Ceram. Soc.* **2014**, *34*, 1375−1385.
(31) Kumar, P. T.; Lakshmanan, V. K.; Anilkumar, T. V.; Ramya, C.; Reshmi, P.; Unnikrishnan, A. G.; Nair, S. V.; Jayakumar, R. Flexible and Microporous Chitosan Hydrogel/Nano ZnO Composite Bandages for Wound Dressing: In Vitro and in Vivo Evaluation. *ACS Appl. Mater. Interfaces* **2012**, *4*, 2618−2629.
(32) Zhu, Y.; Zhang, L.; Wang, L.; Tan, R.; Cao, L. Interface Diffusion and Reaction between TiO2 Film Photocatalyst and Aluminium Alloy Substrate. *Surf. Interface Anal.* **2001**, *1*, 218−223.
(33) Gan, L.; Wang, J.; Pilliar, R. M. Evaluating Interface Strength of Calcium Phosphate Sol−Gel-derived Thin Films to Ti6Al4V Substrate. *Biomaterials* **2005**, *26*, 189−96.
(34) Gittens, R. A.; McLachlan, T.; Olivares-Navarrete, R.; Cai, Y.; Berner, S.; Tannenbaum, R.; Schwartz, Z.; Sandhage, K. H.; Boyan, B. D. The Effects of Combined Micron-/Submicron-Scale Surface Roughness and Nanoscale Features on Cell Proliferationand Differentiation. *Biomaterials* **2011**, *32*, 3395−3403.
(35) Chen, X.; Cai, K.; Lai, M.; Zhao, L.; Tang, L. Mesenchymal Stem Cells Differentiation on Hierarchically Micro/Nano-Structured Titanium Substrates. *Adv. Eng. Mater.* **2012**, *14*, 216−223.
(36) Han, Y.; Chen, D.; Sun, J.; Zhang, Y. UV-Enhanced Bioactivity and Cell Response of Micro-Arc Oxidized Titania Coatings. *Acta. Biomater.* **2008**, *4*, 1518−1529.
(37) Wagner, C. D.; Riggs, W. M.; Davis, L. E.; Moulder, J. F. Chapter II. In *Handbook of X-ray Photoelectron Spectroscopy;* Mulenger, G. E., Ed.; Perkin-Elmer Corp.: Waltham, MA, 1979; pp 29−173.
(38) Cai, K.; Rechtenbach, A.; Hao, J.; Bossert, J.; Jandt, K. D. Polysaccharide-Protein Surface Modification of Titanium via a Layer-by-Layer Technique: Characterization and Cell Behaviour Aspects. *Biomaterials* **2005**, *26*, 5960−5971.
(39) Palza, H.; Escobar, B.; Bejarano, J.; Bravo, D.; Diaz-Dosque, M.; Perez, J. Designing Antimicrobial Bioactive Glass Materials with Embedded Metal Ions Synthesized by the Sol-Gel Method. *Mater. Sci. Eng., C* **2013**, *33*, 3795−3801.
(40) Aina, V.; Perardi, A.; Bergandi, L.; Malavasi, G.; Menabue, L.; Morterra, C.; Ghigo, D. Cytotoxicity of Zinc-Containing Bioactive Glasses in Contact with Human Osteoblasts. *Chem.-Biol. Interact.* **2007**, *167*, 207−218.
(41) Wang, Y. W.; Cao, A.; Jiang, Y.; Zhang, X.; Liu, J. H.; Liu, Y.; Wang, H. Superior Antibacterial Activity of Zinc Oxide/Graphene Oxide Composites Originating from High Zinc Concentration Localized around Bacteria. *ACS Appl. Mater. Interfaces* **2014**, *6*, 2791−2798.
(42) Shen, C.; James, S. A.; de Jonge, M. D.; Turney, T. W.; Wright, P. F.; Feltis, B. N. Relating Cytotoxicity, Zinc Ions, and Reactive Oxygen in ZnO Nanoparticle Exposed Human Iimmune Cells. *Toxicol. Sci.* **2013**, *136*, 120−130.
(43) Raghupathi, K. R.; Koodali, R. T.; Manna, A. C. Size-Dependent Bacterial Growth Inhibition and Mechanism of Antibacterial Activity of Zinc Oxide Nanoparticles. *Langmuir* **2011**, *27*, 4020−4028.
(44) Huo, K.; Zhang, X.; Wang, H.; Zhao, L.; Liu, X.; Chu, P. K. Osteogenic Activity and Antibacterial Effects on Titanium Surfaces Modified with Zn-Incorporated Nanotube Arrays. *Biomaterials* **2013**, *34*, 3467−3478.
(45) Hu, Y.; Cai, K.; Luo, Z.; Xu, D.; Xie, D.; Huang, Y.; Yang, W.; Liu, P. TiO_2 Nanotubes as Drug Nanoreservoirs for the Regulation of Mobility and Differentiation of Mesenchymal Stem Cells. *Acta Biomater.* **2012**, *8*, 439−448.
(46) Farahani, E.; Patra, H. K.; Jangamreddy, J. R.; Rashedi, I.; Kawalec, M.; Rao Pariti, R. K.; Batakis, P.; Wiechec, E. Cell Adhesion Molecules and Their Relation to (Cancer) Cell Stemness. *Carcinogenesis* **2014**, *35*, 747−759.
(47) Wrighton, K. H. Mechanotransduction: Vinculin Discrimination at Adhesions. *Nat. Rev. Mol. Cell Biol.* **2014**, *15*, 367−367.
(48) Hu, Y.; Cai, K.; Luo, Z.; Zhang, Y.; Li, L.; Lai, M.; Hou, Y.; Huang, Y.; Li, J.; Ding, X.; Zhang, B.; Sung, K. L. Regulation of the Differentiation of Mesenchymal Stem Cells in Vitro and Osteogenesis in Vivo by Microenvironmental Modification of Titanium Alloy Surfaces. *Biomaterials* **2012**, *33*, 3515−3528.
(49) Seo, H. J.; Cho, Y. E.; Kim, T.; Shin, H. I.; Kwun, I. S. Zinc May Increase Bone Formation through Stimulating Cell Proliferation, Alkaline Phosphatase Activity and Collagen Synthesis in Osteoblastic MC3T3-E1 Cells. *Nutr. Res. Pract.* **2010**, *4*, 356−361.
(50) Xu, D.; Xu, L.; Zhou, C.; Lee, W. Y.; Wu, T.; Cui, L.; Li, G. Salvianolic Acid B Promotes Osteogenesis of Human Mesenchymal Stem Cells through Activating ERK Signaling Pathway. *Int. J. Biochem. Cell Biol.* **2014**, *51*, 1−9.
(51) Peng, S.; Liu, X. S.; Huang, S.; Li, Z.; Pan, H.; Zhen, W.; Luk, K. D.; Guo, X. E.; Lu, W. W. The Cross-Talk between Osteoclasts and Osteoblasts in Response to Strontium Treatment: Involvement of Osteoprotegerin. *Bone* **2011**, *49*, 1290−1298.
(52) Litsuka, N.; Hie, M.; Tsukamoto, I. Zinc Supplementation Inhibits the Increase in Osteoclastogenesis and Decrease in Osteoblastogenesis in Streptozotocin-Induced Diabetic Rats. *Eur. J. Pharmacol.* **2013**, *714*, 41−47.
(53) Hu, Y.; Cai, K.; Luo, Z.; Jandt, K. D. Layer-by-Layer Assembling β-estradiol Loaded Mesoporous Silica Nanoparticles on Titanium Substrates and Its Implication for Bone Homeostasis. *Adv. Mater.* **2010**, *22*, 4146−4150.
(54) Mladenović, Ž.; Johansson, A.; Willman, B.; Shahabi, K.; Björn, E.; Ransjö, M. Soluble Silica Inhibits Osteoclast Formation and Bone Resorption in Vitro. *Acta. Biomater.* **2014**, *10*, 406−418.
(55) Roy, M.; Fielding, G.; Bandyopadhyay, A.; Bose, S. Effects of Zinc and Strontium Substitution in Tricalcium Phosphate on Osteoclast Differentiation and Resorption. *Biomater. Sci.* **2013**, *1*, 74−82.
(56) Luo, X.; Barbieri, D.; Davison, N.; Yan, Y.; de Bruijn, J. D.; Yuan, H. Zinc in Calcium Phosphate Mediates Bone Induction: In Vitro and in Vivo Model. *Acta. Biomater.* **2014**, *10*, 477−485.
(57) Park, J.; Bauer, S.; Schlegel, K. A.; Neukam, F. W.; von der Mark, K.; Schmuki, P. TiO_2 Nanotube Surfaces: 15 nm-an Optimal Length Scale of Surface Topography for Cell Adhesion and Differentiation. *Small* **2009**, *5*, 666−671.
(58) Zreiqat, H.; Ramaswamy, Y.; Wu, C.; Paschalidis, A.; Lu, Z.; James, B.; Birke, O.; McDonald, M.; Little, D.; Dunstan, C. R. The Incorporation of Strontium and Zinc into a Calcium−Silicon Ceramic for Bone Tissue Engineering. *Biomaterials* **2010**, *31*, 3175−3184.
(59) Cai, K.; Yao, K.; Hou, X.; Wan, Y. Q.; Hou, Y. J.; Yang, Z. M.; Li, X.; Xie, H. Improvement of the Functions of Osteoblasts Seeded on Modified Poly(D,L-lactic acid) with Poly(aspartic acid). *J. Biomed. Mater. Res.* **2002**, *62*, 283−291.
(60) Zhang, W.; Wang, G.; Liu, Y.; Zhao, X.; Zou, D.; Zhu, C.; Jin, Y.; Huang, Q.; Sun, J.; Liu, X.; Jiang, X.; Zreiqat, H. The Synergistic Effect of Hierarchical Micro/Nano-Topography and Bioactive Ions for Enhanced Osseointegration. *Biomaterials* **2013**, *34*, 3184−3195.

(61) Ong, J. L.; Carnes, D. L.; Bessho, K. Evaluation of Titanium Plasma-Sprayed and Plasma-Sprayed Hydroxyapatite Implants in Vivo. *Biomaterials* **2004**, *25*, 4601−4606.